ARTICLE

Synthesis of Multifunctional Composite Microgels *via In Situ* Ni Growth on pNIPAM-Coated Au Nanoparticles

Ana Sánchez-Iglesias,[†] Marek Grzelczak,[†,‡,*] Benito Rodríguez-González,[†] Pablo Guardia-Girós,[§] Isabel Pastoriza-Santos,[†] Jorge Pérez-Juste,[†] Maurizio Prato,[‡] and Luis M. Liz-Marzán[†,*]

[†]Departamento de Química Física and Unidad Asociada CSIC, Universidade de Vigo, 36310 Vigo, Spain, [‡]Dipartimento di Scienze Farmaceutiche, Università degli Studi di Trieste, 34127 Trieste, Italy, and [§]Departament d'Electrònica and Institut de Nanociència i Nanotecnologia, Universitat de Barcelona, c. Martí i Franquès 1, Barcelona 08028, Spain

ABSTRACT Novel colloidal composites have been designed to incorporate multiple functionalities that allow optical detection, magnetic manipulation, molecular trapping, and thermal response. Such particles are made of gold nanoparticle cores covered by a thin layer of metallic nickel and a poly(*N*-isopropylacrylamide) (pNIPAM) shell. While the gold cores provide efficient optical response through localized surface plasmon resonances, nickel allows external magnetic manipulation and the pNIPAM shell can be swollen or collapsed as a function of temperature, thus allowing capture and release of various types of molecules.

KEYWORDS: gold nanoparticles · pNIPAM · nickel · thermosensitive microgels · nanocomposite colloids

After very significant advances have been achieved in the development and fabrication of a wide variety of functional nanomaterials, the scientific community has seen increasing interest in the incorporation of multiple functionalities within individual nanostructures. Such multifunctional nanomaterials can find application, for example, in biomedicine if properties such as labeling, sensing, directed transport, and drug release are combined within the same particle. This field has significantly evolved during the past few years, and colloid synthesis in particular has made important contributions in this direction. For example, magnetic nanoparticles and semiconductor quantum dots were assembled within colloidal particles,[1−3] providing them with magnetic and optical response. Combination of magnetic and metal nanoparticles has also been demonstrated to be useful in sensing applications.[4−6]

A different type of materials that has acquired particular interest in this respect comprises the combination of microgel particles[7−10] with other functional nanomaterials because microgels can be swollen or collapsed under the influence of external stimuli, such as temperature or pH. Among microgel polymers, poly(*N*-isopropylacrylamide) (pNIPAM) has been most often studied, and several examples have been recently reported on the incorporation of various types of nanoparticles, either within the microgel porous network[11−17] or on the microgel surface.[18−22] In these hybrid nanomaterials, the tunable porosity of the microgel can be used for selectively allowing/suppressing the diffusion of certain molecules, which can then react within the microgel (*e.g.*, when nanocatalysts are included),[23] or simply be captured and released at a later stage when the appropriate external switch is triggered.[24−26] We have recently reported[27] a synthetic method that allowed us to directly grow thermosensitive pNIPAM on the surface of gold nanoparticles, thus providing the microgel with well-defined optical response due to the characteristic surface plasmon resonance (SPR) of the gold cores. Interestingly, the SPR wavelength was found to be highly sensitive toward the refractive index changes occurring during the temperature-driven swelling and collapse of the microgel, associated with a volume phase transition. We have additionally demonstrated[24] that such core−shell colloids can be used to trap different types of molecules, which can be detected *in situ* by means of surface-enhanced Raman scattering (SERS). However, despite a few recent reports,[28,29] the uniform incorporation of a magnetic component within microgels is still very poorly developed, and the strategies proposed so far include either growth of the microgel on the surface of silica colloids containing magnetic nanocrystals[30] or capture of magnetic nanocrystals directly within or at the surface of the microgel network.[31−34] Building upon our prior ex-

*Address correspondence to mgrzelczak@units.it, lmarzan@uvigo.es.

Received for review June 11, 2009 and accepted September 9, 2009.

Published online September 21, 2009. 10.1021/nn9006169 CCC: $40.75

perience in the growth of pNIPAM on gold nanoparticles, we report here a novel method to provide them with magnetic functionality, through controlled growth of a nickel shell on the encapsulated gold nanoparticles, while maintaining the optical response of the gold cores and the thermoresponsive properties of the microgel.

RESULTS AND DISCUSSION

The preparation of these novel multicomponent, multifunctional nanoparticles is based on a combination of several methods previously developed in our group. On one hand, we have recently reported the buildup of thermosensitive pNIPAM shells on CTAB-capped gold spheres, as well as the subsequent growth of the gold core by the further catalytic reduction of gold salt, upon diffusion through the porous polymeric shell.[27] On the other hand, we have been able to coat various types of nanomaterials, including gold nanoparticles, with uniform nickel shells, through Pt-catalyzed hydrazine reduction of $NiCl_2$.[35] These two different procedures can be combined in such a way that Ni shells are grown on the surface of gold spheres which have been previously surrounded by the porous pNIPAM microgel, so that a magnetic component can be added to the optically and thermally responsive Au@pNIPAM colloids. The growth of Ni on Au was reported to proceed only if a small amount of Pt was present on the particle surface,[35] which would act as a catalyst for decomposition of a Ni−hydrazine complex. This was also confirmed in the present study (not shown control experiments evidenced that Ni could not be grown on pure Au cores), and therefore, prior to growth of the Ni shell, the Au cores had to be covered with a small amount of Pt. This was achieved through addition of K_2PtCl_4, CTAB, and ascorbic acid, so that both the Pt^{2+}−CTAB complex and ascorbic acid diffuse through the porous pNIPAM shell and catalytic reduction occurs at the gold core surface. (In the absence of the Au cores, no Pt(II) reduction takes place under these conditions.) Subsequently, the Pt layer can be used as a catalyst for growth of a Ni shell through decomposition of Ni−hydrazine complexes at 35 °C, which was previously found to be the optimal temperature for this process.[36] Again, in the absence of the Pt layer, no Ni(II) reduction could be achieved.

Although both reactions were carried out at 35 °C, a temperature slightly above the lower critical solution temperature (LCST), microgel collapse was not found to significantly hinder the diffusion of reactants through the shell. Working above the LCST involves reduction of the microgel porosity, leading to a slower diffusion rate of the Pt^{2+}−CTAB or the Ni^{2+}−hydrazine complexes through the polymer shell. Since a decreased reduction rate was expected at higher temperature, a compromise temperature of 35 °C was chosen to avoid complete collapse of the microgel but still high enough

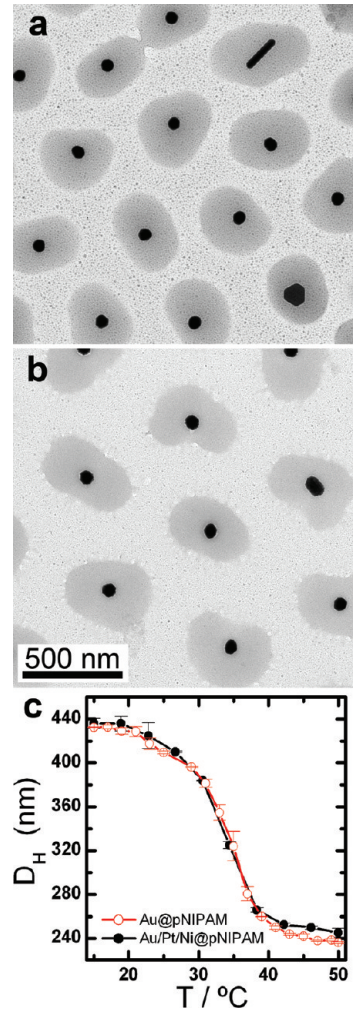

Figure 1. TEM micrographs showing gold nanoparticles coated with pNIPAM before (a) and after (b) nickel reduction. (c) Variation of the hydrodynamic diameter of Au@pNIPAM (open circles) and Au/Pt/Ni@pNIPAM (solid circles) with temperature, showing no changes of microgel diameter before and after growth of Pt and Ni.

to promote Ni(II) reduction. Careful choice of the experimental conditions was crucial to achieve the optimal thickness of both the Pt and Ni shells, which maintained optical activity and imparted significant magnetic response. We found that the thickness of the Ni shell (Figure S1 in the Supporting Information) could be controlled by adjusting hydrazine concentration as indicated in the Experimental Section, while lower $NiCl_2$ concentrations did not yield uniform Ni shells and higher concentrations resulted into non-uniform growth or fully damped SPR. As shown in Figure 1 for the initial and final states, both the appearance of the particles in the low magnification TEM images and the measured average overall particle size were not significantly affected during the whole process.

However, through higher resolution TEM and EDS microanalysis, it was demonstrated that the cores did indeed change after each individual step (see Figure 2 and Supporting Information S2). First of all, for the Pt-modified Au cores, prior to Ni reduction, EDS microanal-

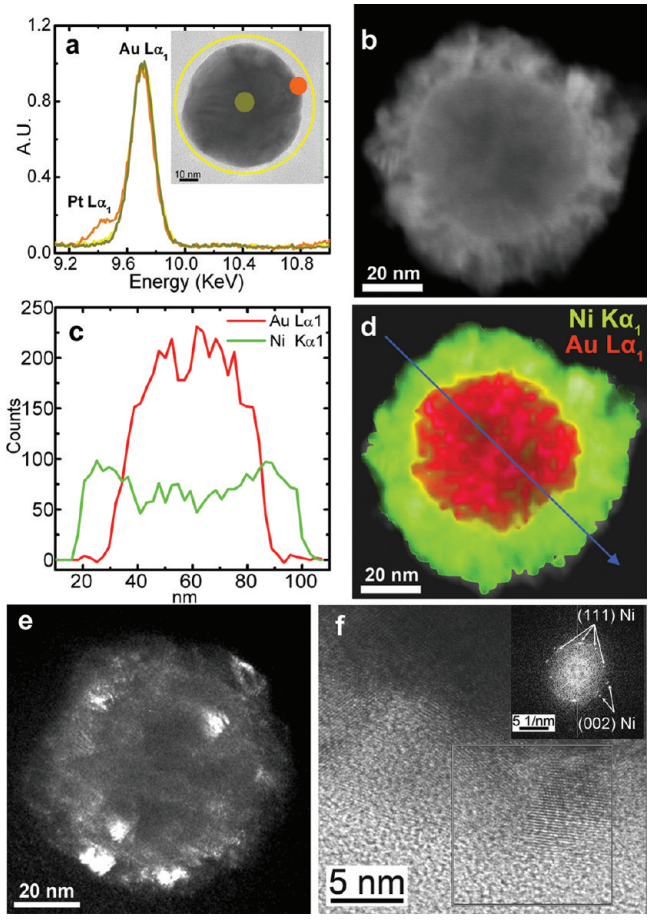

Figure 2. (a) EDS spectra of Au/Pt@pNIPAM taken from different areas of one particle, showing detectable presence of metallic platinum at the edges. (b) Dark field STEM image of a single Au/Pt@Ni core showing typical core/shell structure. (c) STEM-XEDS line scans across the particle shown in b, for Au and Ni. (d) STEM-XEDS RGB image (Au = red; Ni = green), with an arrow indicating the profile line (c). (e) Dark field TEM image of a Au/Pt@Ni core with a thinner Ni shell, and (f) HRTEM image of the polycrystalline Ni shell (the FFT image from the marked area is shown in the inset).

ysis at the center and the edge of a single core (Figure 2a) undoubtedly shows the presence of Pt at the particles' surface, whereas Au predominates at the central area of the particle. Additionally, both bright field and dark field images of the cores obtained after Ni reduction revealed the presence of a rough shell uniformly covering the Au spheres. Line profile microanalysis across a single core (Figure 2c) showed that the shell is made of Ni, whereas, again, Au was the predominant element at the particle center. Complete STEM-XEDS mapping was also carried out on the whole particle (Figure 2d), providing elemental distribution, which agrees with the expected core−shell structure, also observed in the dark field HAADF STEM image (Figure 2b). This is thus a demonstration that the coating process did indeed proceed as expected, so that Ni was grown on each individual Au core, without apparently affecting the corresponding pNIPAM shell. As reported for similar systems,[35,36] these shells are expected to comprise an inner metallic Ni layer, surrounded by an external layer of Ni oxide/hydroxide, which explains the outermost roughness. Evidence of the polycrystalline structure of the Ni shell was provided by analysis of a different sample with a smaller shell thickness (*ca.* 4 nm). The random orientation of the polycrystalline shell originates bright spots in the TEM dark field image shown in Figure 2e, whereas the HRTEM image in Figure 2f clearly reveals well-resolved lattice planes, which can be assigned to face centered cubic nickel. The different orientations of adjacent grains are also reflected in the corresponding fast Fourier transformed (FFT) image shown in the inset.

The beauty of this system, which differentiates it from other examples of nanoparticle-loaded microgel colloids, is the combination of a number of different functions that are interesting in themselves but become even more interesting when combined within a single nano-object. It is thus crucial to characterize not only the thermosensitive volume change of the pNIPAM shell (shown in Figure 1c) but also the optical (related to the surface plasmon resonance, SPR, of the Au cores) and magnetic (related to the Ni/NiO shells) properties of these composite colloids. The optical response was characterized through standard UV−vis spectroscopy in aqueous solution. Spectra were thus recorded during the various steps of the coating, as shown in Figure 3a. In fact, we feared that the SPR band, originally present in the Au@pNIPAM colloids, could be completely screened when the cores became covered with the Ni shells, as previously reported for Au nanorods.[35] Although damping of the SPR band was indeed observed upon Pt coating, and even more strongly upon Ni coating, a well-defined SPR band could still be recorded, which was significantly (*ca.* 20 nm) red-shifted as compared to the original one, as also reflected in an obvious color change observed during the process. Theoretical modeling based on the boundary element method (see Experimental Section and Supporting Information for details) was carried out using a multilayer model that intended to reproduce the experimental system as closely as possible, as depicted in Figure S3 (Supporting Information). The thickness of each layer in the core was estimated from statistical analysis of particle size from TEM images at each synthesis step (see size distributions in the Supporting Information, Figure S1), while the thickness of the organic pNIPAM shell was determined from DLS measurements, as shown in Figure 1c. For Au, Pt, and Ni, experimental, wavelength-dependent dielectric data were used, but for NiO and pNIPAM, constant values were chosen for simplicity and proven to yield meaningful results. As can be observed in Figure 3a,b, the agreement between experimental and calculated spectra is not only remarkably good for the initial Au@pNIPAM-coated spheres but also the theoretical results faithfully reproduce the experimental trend upon deposition of the Pt and Ni/NiO shells, confirming that the observed, broadened plasmon

band for the Ni-coated Au cores is not a result of incomplete coating, but indeed corresponds to the expected core−multishell morphology. Additionally, when the UV−vis spectra were recorded for both colloids (Au@pNIPAM and Au@Ni@pNIPAM) at low and high temperature (below and above the LCST), a significant shift of the SPR band was observed (Figure 3c), and again, theoretical modeling (using estimated refractive index values of 1.335 and 1.414 for the expanded and collapsed microgels, respectively) was in agreement with the experimental trend (Figure 3d). While plasmon shifts upon compression have been reported for various Au@pNIPAM systems,[19,27] it is interesting that the refractive index sensitivity is preserved when the Ni/NiO shell surrounds the Au cores, meaning that the Ni shell is not sufficiently thick to fully screen the optical sensitivity of the cores. Apart from the obvious interest for direct environmental sensing using the particles in solution, we can additionally foresee future applications in the biosensing area if the optical and magnetic properties can be combined, so that contributions toward magnetoplasmonic biosensing[37,38] can be envisaged.

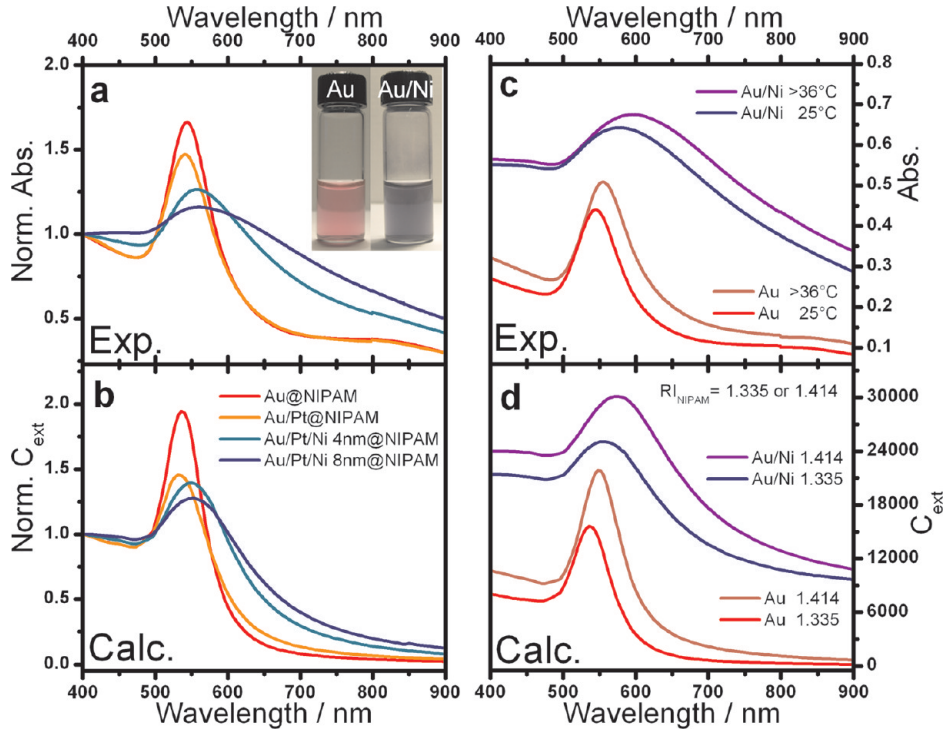

Figure 3. Left panel: Optical characterization and modeling of Au/Pt/Ni@pNIPAM colloids. Experimental (a) and calculated (b) spectra for the four different growth steps, as indicated. The inset in (a) shows digital images of the colloid before and after nickel growth. Right panel: Experimental (c) and calculated (d) spectra for Au@pNIPAM and Au/Pt/Ni@pNIPAM at temperatures below and above the LCST (see Experimental Section for details).

However, this obviously requires a significant magnetic response of the Ni shell. Previous studies for similar systems[36,39,40] have demonstrated that Ni/NiO shells and nanoparticles grown using the Pt-catalyzed reduction of Ni^{2+} with hydrazine are typically ferromagnetic and readily respond to external magnetic fields. In spite of the small thickness of the Ni shells deposited in the present study, the composite colloidal spheres were also observed to respond toward an applied external magnetic field, even at room temperature. This is exemplified in Figure 4. Shown in Figure 4a,b are low magnification TEM images of Au@Ni@pNIPAM spheres, which were dried on carbon-coated TEM grids in the absence (a) and in the presence (b) of an external magnetic field. Obviously, when no magnetic field was applied, the distribution of the particles on the grid was homogeneous, while in the presence of a low intensity magnetic field, there is preferential alignment of the particles along the magnetic field lines, as has been repeatedly reported for a variety of magnetic nanoparticle systems. This is a first demonstration of the magnetic character of the particles at room temperature, which is confirmed by the photographs in Figure 4c, showing the uniform dispersion of par-

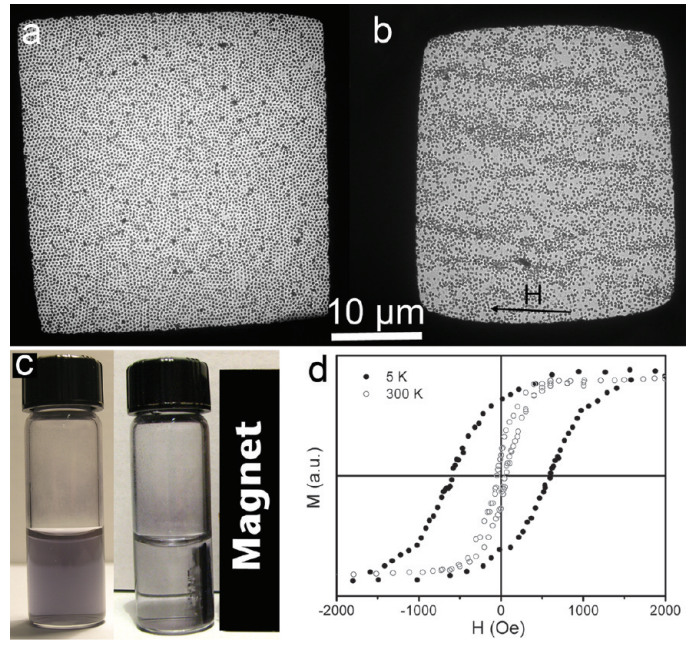

Figure 4. (a,b) TEM images of samples dried on a TEM grid under zero (a) and low intensity (0.2 T) (b) magnetic field. (c) Digital photographs of a nanocomposite colloid before (left) and after (right) placing a permanent magnet next to it. (d) Hysteresis loops at 5 and 300 K showing typical ferromagnetic behavior of the sample (see Supporting Information Figure S4 for the complete hysteresis loops).

ticles in the colloid, which is completely lost, when a hand-held magnet is placed next to the vial, which was able to drag all the particles toward it within 1 h because of magnetic attraction. While a detailed analysis of the magnetic properties is out of the scope of this paper, we show in Figure 4d the low magnetic field region of a magnetization cycle for the dried colloid recorded at low (5 K) and high (300 K) temperature (full cycles showing complete saturation at high field are shown in the Supporting Information, Figure S4). In both cases, the loops present hysteresis, revealing the ferromagnetic nature of this system.[41,42] It should be noted that, as opposed to most measurements on nanoparticle systems, in this case, interparticle interactions can be completely neglected since even in the dry state there is a significant separation between cores, dictated by the pNIPAM shells. Zero field cooling-field cooling (ZFC-FC) magnetization measurements (see Figure S5 in the Supporting Information) show a blocking temperature above room temperature, in agreement with the hysteresis of the sample at room temperature.

CONCLUSIONS

Multifunctional nanomaterials were fabricated through a rational design and modification through colloid chemistry methods. We have demonstrated the preparation of thermoresponsive pNIPAM microgels containing optically active gold nanoparticles, surrounded by magnetically responsive nickel shells. These nanocomposite colloids can be readily manipulated through external magnetic fields and show optical response that is highly sensitive toward refractive index changes such as those induced by collapse and swelling of the pNIPAM shell. This type of material can open new possibilities toward applications in controlled molecular uptake and release where detection and external manipulation are possible.

EXPERIMENTAL SECTION

Chemicals. Ascorbic acid, cetyltrimethylammonium bromide (CTAB), $HAuCl_4 \cdot 3H_2O$, K_2PtCl_4, $NiCl_2$, hydrazine monohydrate 98%, trisodium citrate dihydrate, styrene, divinylbenzene, *N*-isopropylacrylamide, and *N*,*N*-methylenebisacrylamide were supplied by Aldrich. 2,2′-Azobis(2-methylpropionamidine) dihydrochloride was supplied by Acros. All reactants were used without further purification. Water was milli-Q grade.

Synthesis of CTAB-Stabilized Gold Spheres. Gold nanoparticles were prepared through a previously reported seeded growth method.[43] Briefly, gold seeds (15 nm, 0.5 mM) were prepared by citrate reduction[44] and then diluted with the same volume of a 30 mM CTAB solution. Seeded growth was carried out by addition of ascorbic acid solution (0.5 mM) onto a mixture of $HAuCl_4$ (0.25 mM) and CTAB (15 mM) at 35 °C, followed by addition of the seed solution ([Au] = 4.47 μM).

Encapsulation of Gold Spheres in pNIPAM Shell. Encapsulation of gold nanoparticles in thermoresponsive pNIPAM microgels involves several steps.[27] Initial polystyrene coating was performed as follows: 150 mL of as-prepared CTAB-stabilized gold nanoparticles was centrifuged at 4500 rpm for 40 min, the supernatant discarded, and the precipitate redispersed in 150 mL of milli-Q water. The solution was then heated to 30 °C, followed by addition of styrene (10 μL) and divinylbenzene (5 μL) under stirring. After 15 min, the temperature was raised to 70 °C and polymerization was initiated by adding 2,2′-azobis(2-methylpropionamidine)dihydrochloride (20 μL 100 mM in water). The polymerization was allowed to proceed for 2 h. The solution was centrifuged once at 4000 rpm (40 min), the supernatant discarded, and the precipitate redispersed in 15 mL of milli-Q water. The solution was purged with nitrogen (15 min at 70 °C), followed by addition of *N*-isopropylacrylamide (0.1698 g) and *N*,*N*-methylenebisacrylamide (0.0234 g). After 15 min, the nitrogen flow was removed and polymerization was initiated by addition of 2,2′-azobis(2-methylpropionamidine)dihydrochloride (150 μL 100 mM). After 7−10 min, the colorless solution became turbid, and the reaction was allowed to proceed for 2 h at 70 °C. The pink milky mixture was then allowed to cool to room temperature under stirring. To remove small oligomers, unreacted monomers, as well as gold-free microgels, the dispersion was diluted with water (15 mL) and washed three times by centrifugation (30 min, 4000 rpm) and redispersion in water (5 mL).

Catalytic Growth of Nickel/Nickel Oxide Shell on Platinum-Coated Gold Surface. An initial, catalytic Pt shell was grown as follows: K_2PtCl_4 (0.25 mL, 10 mM) was added to 25 mL of CTAB 100 mM, and the mixture was incubated at 35 °C for 30 min to allow for complexation of platinum with CTAB, followed by addition of ascorbic acid (0.875 mL, 100 mM). To this solution was added an appropriate amount of Au@pNIPAM, keeping the Au^0/Pt^{II} molar ratio equal to 1.6. The mixture was stored at 35 °C for 24 h, followed by three-fold washing (4000 rpm, 30 min) and redispersion in 2 mL of water. For Ni reduction, 40 μL of 250 mM $NiCl_2$, 448 μL of 2 M hydrazine, and 2 mL of Au/Pt@NIPAM were added to 22.5 mL of water at 35 °C, under sonication. This mixture was left for 6 h at 35 °C, followed by three-fold centrifugation (3500 rpm, 30 min) and redispersion in 5 mL of water. The resulting Ni/NiO shell was 8 nm thick on average (from TEM). Thinner Ni/NiO shells (4 nm) were obtained by reducing by half the amount of hydrazine, keeping volumes and concentrations of all other compounds unchanged.

Magnetophoretic Deposition. The nanocomposite solution was drop-casted on the TEM copper grid at 300 K between two permanent magnets, providing a magnetic field of 0.2 T.

Characterization. Optical characterization was carried out by UV−vis−NIR spectroscopy with a Cary 5000 spectrophotometer, using 1 mm path length quartz cuvettes. Transmission electron microscopy (TEM) images were obtained with a JEOL JEM 1010 transmission electron microscope operating at an acceleration voltage of 100 kV, while high resolution TEM (HRTEM) and analytical STEM studies were performed with a JEOL JEM 2010 FEG-TEM operating at an acceleration voltage of 200 kV. X-ray energy-dispersive spectra (EDS) were acquired using an Inca Energy 200 TEM system from Oxford Instruments, and elemental maps (STEM-XEDS) were acquired coupling the X-ray spectrometer to a STEM unit, equipped with a high angle annular dark field detector (HAADF). Mapping was performed with 0.7 nm probe size and 40 cm camera length. Background subtraction was carried out prior to mapping overlap. Zeta potential and hydrodynamic diameters were measured using a Zetasizer Nano S (Malvern Instruments, Malvern, UK). Field- and temperature-dependent magnetic measurements were performed on the dried coated particles, at 5 and 300 K, up to 5 T, in a V10 Quantum Design SQUID magnetometer.

Modeling of Optical Properties. Simulations of optical spectra were based on the boundary element method (BEM),[45,46] for concentric, multishell spheres made of dielectric media representing gold, platinum, nickel, pNIPAM, and water as solvent with dimensions estimated from the experimental results (see schematic drawings in the Supporting Information). The dielectric data for Au were taken from Johnson and Christy,[47] for Pt

and Ni from Palik,[48] for NiO from ref 49, and constant values of 1.335 and 1.414 were taken for the expanded and collapsed microgel shell, respectively.[50]

Acknowledgment. L.M.L.-M. acknowledges financial support from the Spanish Ministerio de Ciencia e Innovación (MAT2007-62696 and Consolider Ingenio 2010, CSD2006-12, NANO-BIOMED) and from the EU (NANODIRECT, Grant No. CP-FP 213948-2).

Supporting Information Available: Size distributions, EDS spectra, models for BEM calculations, and magnetization curves. This material is available free of charge *via* the Internet at http://pubs.acs.org.

REFERENCES AND NOTES

1. Medintz, I.; Uyeda, H. T.; Goldman, E. R.; Mattoussi, H. Quantum Dot Bioconjugates for Imaging, Labelling and Sensing. *Nat. Mater.* **2005**, *4*, 436–446.
2. Salgueiriño-Maceira, V.; Correa-Duarte, M. A. Increasing the Complexity of Magnetic Core/Shell Structured Nanocomposites for Biological Applications. *Adv. Mater.* **2007**, *19*, 4131–4144.
3. Cozzoli, P. D.; Pellegrino, T.; Manna, L. Synthesis, Properties and Perspectives of Hybrid Nanocrystal Structures. *Chem. Soc. Rev.* **2006**, *35*, 1195–1208.
4. Piao, Y.; Burns, A.; Kim, J.; Wiesner, U.; Hyeon, T. Designed Fabrication of Silica-Based Nanostructured Particle Systems for Nanomedicine Applications. *Adv. Funct. Mater.* **2008**, *18*, 3745–3758.
5. Wang, C.; Xu, C.; Zeng, H.; Sun, S. Recent Progress in Syntheses and Applications of Dumbbell-like Nanoparticles. *Adv. Mater.* **2009**, *21*, 3045–3052.
6. Spuch-Calvar, M.; Rodríguez-Lorenzo, L.; Morales, M. P.; Alvarez-Puebla, R. A.; Liz-Marzán, L. M. Bifunctional Nanocomposites with Long-Term Stability as SERS Optical Accumulators for Ultrasensitive Analysis. *J. Phys. Chem. C* **2009**, *113*, 3373–3377.
7. Pich, A. Z.; Adler, H.-J. P. Composite Aqueous Microgels: an Overview of Recent Advances in Synthesis, Characterization and Application. *Polym. Int.* **2007**, *56*, 291–307.
8. Ballauff, M.; Borisov, O. Polyelectrolyte Brushes. *Curr. Opin. Colloid Interface Sci.* **2006**, *11*, 316–323.
9. Das, M.; Zhang, H.; Kumacheva, E. Microgels: Old Materials with New Applications. *Ann. Rev. Mater. Res.* **2006**, *36*, 117–142.
10. Pelton, R. Temperature-Sensitive Aqueous Microgels. *Adv. Colloid Interface Sci.* **2000**, *85*, 1–33.
11. Kim, J.-H.; Lee, T. R. Thermo- and pH-Responsive Hydrogel-Coated Gold Nanoparticles. *Chem. Mater.* **2004**, *16*, 3647–3651.
12. Lu, Y.; Mei, Y.; Drechsler, M.; Ballauff, M. Thermosensitive Core−Shell Particles as Carriers for Ag Nanoparticles: Modulating the Catalytic Activity by a Phase Transition in Networks. *Angew. Chem., Int. Ed.* **2005**, *45*, 813–816.
13. Lu, Y.; Mei, Y.; Ballauff, M.; Drechsler, M. Thermosensitive Core−Shell Particles as Carrier Systems for Metallic Nanoparticles. *J. Phys. Chem. B* **2006**, *110*, 3930–3937.
14. Zhang, J.; Xu, S.; Kumacheva, E. Photogeneration of Fluorescent Silver Nanoclusters in Polymer Microgels. *Adv. Mater.* **2005**, *17*, 2336–2340.
15. Suzuki, D.; Kawaguchi, H. Gold Nanoparticle Localization at the Core Surface by Using Thermosensitive Core−Shell Particles as a Template. *Langmuir* **2005**, *21*, 12016–12024.
16. Singh, N.; Lyon, L. A. Au Nanoparticle Templated Synthesis of pNIPAM Nanogels. *Chem. Mater.* **2007**, *19*, 719–726.
17. Kawano, T.; Niidome, Y.; Mori, T.; Katayama, Y.; Niidome, T. PNIPAM Gel-Coated Gold Nanorods for Targeted Delivery Responding to a Near-Infrared Laser. *Bioconjugate Chem.* **2009**, *20*, 209–212.
18. Gorelikov, I.; Field, L. M.; Kumacheva, E. Hybrid Microgels Photoresponsive in the Near-Infrared Spectral Range. *J. Am. Chem. Soc.* **2004**, *126*, 15938–15939.
19. Das, M.; Sanson, N.; Fava, D.; Kumacheva, E. Microgels Loaded with Gold Nanorods: Photothermally Triggered Volume Transitions under Physiological Conditions. *Langmuir* **2007**, *23*, 196–201.
20. Karg, M.; Pastoriza-Santos, I.; Pérez-Juste, J.; Hellweg, T.; Liz-Marzán, L. M. Nanorod-Coated PNIPAM Microgels: Thermoresponsive Optical Properties. *Small* **2007**, *3*, 1222–1229.
21. Kim, J.-H.; Lee, T. R. Hydrogel-Templated Growth of Large Gold Nanoparticles: Synthesis of Thermally Responsive Hydrogel−Nanoparticle Composites. *Langmuir* **2007**, *23*, 6504–6509.
22. Das, M.; Mordoukhovski, L.; Kumacheva, E. Sequestering Gold Nanorods by Polymer Microgels. *Adv. Mater.* **2008**, *20*, 2371–2375.
23. Schrinner, M.; Proch, S.; Mei, Y.; Kempe, R.; Miyajima, N.; Ballauff, M. Stable Bimetallic Gold−Platinum Nanoparticles Immobilized on Spherical Polyelectrolyte Brushes: Synthesis, Characterization, and Application for the Oxidation of Alcohols. *Adv. Mater.* **2008**, *20*, 1928–1933.
24. Alvarez-Puebla, R.; Contreras-Cáceres, R.; Pastoriza-Santos, I.; Pérez-Juste, J.; Liz-Marzán, L. M. Au@pNIPAM Colloids as Molecular Traps for Surface-Enhanced, Spectroscopic, Ultra-Sensitive Analysis. *Angew. Chem., Int. Ed.* **2009**, *48*, 138–143.
25. Kuang, M.; Wang, D.; Bao, H.; Gao, M.; Möhwald, H.; Jiang, M. Fabrication of Multicolor-Encoded Microspheres by Tagging Semiconductor Nanocrystals to Hydrogel Spheres. *Adv. Mater.* **2005**, *17*, 267–270.
26. Nolan, C. M.; Gelbaum, L. T.; Lyon, L. A. ^{1}H-NMR Investigation of Thermally Triggered Insulin Release from Poly(*N*-isopropylacrylamide) Microgels. *Biomacromolecules* **2006**, *7*, 2918–2922.
27. Contreras-Cáceres, R.; Sánchez-Iglesias, A.; Karg, M.; Pastoriza-Santos, I.; Pérez-Juste, J.; Pacifico, J.; Hellweg, T.; Fernández-Barbero, A.; Liz-Marzán, L. M. Encapsulation and Growth of Gold Nanoparticles in Thermoresponsive Microgels. *Adv. Mater.* **2008**, *20*, 1666–1670.
28. Zhang, F.; Wang, C.-C. Preparation of P(NIPAM-*co*-AA) Microcontainers Surface-Anchored with Magnetic Nanoparticles. *Langmuir* **2009**, *25*, 8255–8262.
29. Chen, L.-B.; Zhang, F.; Wang, C.-C. Rational Synthesis of Magnetic Thermosensitive Microcontainers as Targeting Drug Carriers. *Small* **2009**, *5*, 621–628.
30. Ge, J.; Huynh, T.; Hu, Y.; Yin, Y. Hierarchical Magnetic/Silica Nanoassemblies as Magnetically Recoverable Catalyst Supports. *Nano Lett.* **2008**, *8*, 931–934.
31. Wong, J. E.; Gaharwar, A. K.; Müller-Schulte, D.; Bahadur, D.; Richtering, W. Layer-by-Layer Assembly of a Magnetic Nanoparticle Shell on a Thermoresponsive Microgel Core. *J. Magn. Magn. Mater.* **2007**, *331*, 219–223.
32. Wong, J. E.; Gaharwar, A. K.; Müller-Shulte, D.; Bahadur, D.; Richtering, W. Dual-Stimuli Responsive pNIPAM Microgel Achieved *via* Layer-by-Layer Assembly: Magnetic and Thermoresponsive. *J. Colloid Interface Sci.* **2008**, *324*, 47–54.
33. Rubio-Retama, J.; Zafeiropoulos, N. E.; Serafinelli, C.; Rojas-Reyna, R.; Voit, B.; López-Cabarcos, E.; Stamm, M. Synthesis and Characterization of Thermosensitive pNIPAM Microgels Covered with Superparamagnetic γ-Fe_2O_3 Nanoparticles. *Langmuir* **2007**, *23*, 10280–10285.
34. Kim, J.-W.; Fernández-Nieves, A.; Dan, N.; Utada, A. S.; Marquez, M.; Weitz, D. A. Colloidal Assembly Route for Responsive Colloidosomes with Tunable Permeability. *Nano Lett.* **2007**, *7*, 2876–2880.
35. Grzelczak, M.; Rodríguez-González, B.; Pérez-Juste, J.; Liz-Marzán, L. M. Quasi-Epitaxial Growth of Ni Nanoshells on Au Nanorods. *Adv. Mater.* **2007**, *19*, 2262–2266.
36. Grzelczak, M.; Pérez-Juste, J.; Rodríguez-González, B.; Spasova, M.; Barsukov, I.; Farle, M.; Liz-Marzán, L. M. Pt-Catalyzed Growth of Ni Nanoparticles in Aqueous CTAB Solution. *Chem. Mater.* **2008**, *20*, 5399–5405.
37. Sepúlveda, B.; Calle, A.; Lechuga, L. M.; Armelles, G. Highly Sensitive Detection of Biomolecules with the Magneto-

Optic Surface-Plasmon Resonance Sensor. *Opt. Lett.* **2006**, *31*, 1085–1087.
38. González-Díaz, J. B.; García-Martín, A.; García-Martín, J. M.; Cebollada, A.; Armelles, G.; Sepúlveda, B.; Alaverdyan, Y.; Käll, M. Plasmonic Au/Co/Au Nanosandwiches with Enhanced Magneto-optical Activity. *Small* **2008**, *4*, 202–205.
39. Grzelczak, M.; Correa-Duarte, M. A.; Salgueiriño-Maceira, V.; Rodríguez-González, B.; Rivas, J.; Liz-Marzán, L. M. Pt-Catalyzed Formation of Ni Nanoshells on Carbon Nanotubes. *Angew. Chem., Int. Ed.* **2007**, *46*, 7026–7030.
40. Salgueiriño-Maceira, V.; Correa-Duarte, M. A.; Bañobre-López, M.; Grzelczak, M.; Farle, M.; Liz-Marzán, L. M.; Rivas, J. Magnetic Properties of Ni/NiO Nanowires Deposited onto CNT/Pt Nanocomposites. *Adv. Funct. Mater.* **2008**, *18*, 616–621.
41. Frankamp, B. L.; Boal, A. K.; Tuominen, M. T.; Rotello, V. M. Direct Control of the Magnetic Interaction between Iron Oxide Nanoparticles through Dendrimer-Mediated Self-Assembly. *J. Am. Chem. Soc.* **2005**, *127*, 9731–9735.
42. Johnston-Peck, A. C.; Wang, J.; Tracy, J. B. Synthesis and Structural and Magnetic Characterization of Ni(Core)/NiO(Shell) Nanoparticles. *ACS Nano* **2009**, *3*, 1077–1084.
43. Rodríguez-Fernández, J.; Pérez-Juste, J.; García De Abajo, F. J.; Liz-Marzán, L. M. Seeded Growth of Submicron Au Colloids with Quadrupole Plasmon Resonance Modes. *Langmuir* **2006**, *22*, 7007–7010.
44. Enüstün, B. V.; Turkevich, J. Coagulation of Colloidal Gold. *J. Am. Chem. Soc.* **1963**, *85*, 3317–3328.
45. García De Abajo, F. J.; Howie, A. Retarded Field Calculation of Electron Energy Loss in Inhomogeneous Dielectrics. *Phys. Rev. B* **2002**, *65*, 115418-1–115418-17.
46. Myroshnychenko, V.; Rodríguez-Fernández, J.; Pastoriza-Santos, I.; Funston, A. M.; Novo, C.; Mulvaney, P.; Liz-Marzán, L. M.; García De Abajo, F. J. Modelling the Optical Response of Gold Nanoparticles. *Chem. Soc. Rev.* **2008**, *37*, 1792–1805.
47. Johnson, P. B.; Christy, R. W. Optical Constants of the Noble Metals. *Phys. Rev. B* **1972**, *6*, 4370–4379.
48. Palik, E. D. *Tables from the Handbook of Optical Constants of Solids*; Academic Press: New York, 1995; Vols. 1,2.
49. Powell, R. J.; Spicer, W. E. Optical Properties of NiO and CoO. *Phys. Rev. B* **1970**, *2*, 2182–2193.
50. Garner, B. W.; Cai, T.; Ghosh, S.; Hu, Z.; Neogi, A. Refractive Index Change Due to Volume-Phase Transition in Polyacrylamide Gel Nanospheres for Optoelectronics and Bio-photonics. *Appl. Phys. Express* **2009**, *2*, 057001-4.